"The Anomalous Behavior of Cesium in the Electrical Double Layer: an In-Situ X-ray Spectroscopy Study on Graphene"

Lorenz J. Falling[1,2], Maximilian Jaugstetter[1], Xiao Zhao[1,3], Gustavo Zottis Girotto[2,4], Virginia Altoe[5], Matthijs A. Spronsen[6], Slavomir Nemsak[2]* and Miquel B. Salmeron[1]*

x contributed equally.

* corresponding author

1 Materials Science Division, Lawrence Berkeley National Laboratory, Berkeley, California 94720, United States

2 The Advanced Light Source, Lawrence Berkeley National Laboratory, Berkeley, California 94720, United States

3 Department of Materials Science and Engineering, Stanford University, Stanford, CA 94305, USA

4 Instituto de Física, Universidade Federal do Rio Grande do Sul (UFRGS), Porto Alegre, RS, Brazil

5 The Molecular Foundry, Lawrence Berkeley National Laboratory, Berkeley, California 94720, United States

6 Diamond Light Source Ltd, Oxfordshire, United Kingdom

Graphical abstract:

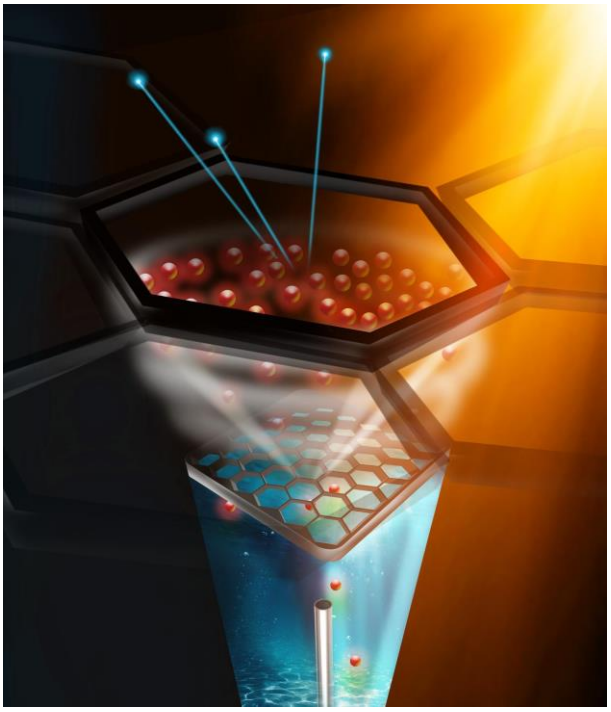

Abstract

Understanding the behavior of ions at electrified interfaces is crucial for the vast majority of electrochemical processes, including energy storage, corrosion, and catalysis. The electric double layer (EDL), formed at the interface between an electrode and an electrolyte, plays a pivotal role in governing these processes. In particular, large ions with a weak charge, such as cesium, exhibit extraordinary behaviors in the EDL, rendering these ions a means to manipulate EDL properties such as solvation, potential drop and local hydrophilicity. In this study, we utilize X-ray and electron transmissive graphene electrodes to investigate the influence of cesium-ions within the EDL using advanced X-ray spectroscopy techniques. By employing synchrotron-based operando X-ray photoelectron spectroscopy (XPS) and electron yield X-ray absorption spectroscopy (XAS), we determine the ion concentrations and elucidate the electronic structure and chemical environment of cesium-ions near the electrode surface. Our results reveal intricate ion-specific interactions within the EDL, shedding light on ion adsorption, desorption, and redistribution phenomena, in dependence of the interfacial cesium concentration. Furthermore, we explore the impact of electrolyte bulk processes, such as ion pairing and surface charge density on the EDL structure and dynamics. Understanding this ion behavior in the EDL is vital for designing electrochemical processes from the electrolyte side. Ease in applicability, high degree of control and dynamic manipulation of this approach, renders it vital for the electrochemistry driven energy revolution.

Introduction

The molecular behavior of solvated species at electrolyte/electrode interfaces is dictated by the electrical double layer (EDL)[1]. This EDL is a response of the mobile electrolyte to screen the surface charge of the solid part of the electrode, ruled by electrostatic effects. The EDL is mathematically described by the Helmholtz model and Gouy-Chapman models[2]. The Gouy-Chapman model provides a theoretical framework for understanding the electrical double layer at charged interfaces and has been foundational in colloid and surface science[3,4]. It assumes a diffuse layer of ions surrounding a charged surface, with ions distributed according to Boltzmann statistics, and predicts the distribution of ions in solution and their influence on surface charge[5]. Despite its utility, the model has limitations in accounting for specific ion-surface interactions, neglecting ion correlations, and may not fully capture the behavior of highly concentrated electrolytes[6]. The implicit accumulation of ions at the interface influences critical parameters of the electrolyte such as the Debye screening length, viscosity, and hydrophilicity. Due to this influence, the nature of the EDL decides over the success of a material as catalyst in electrochemistry or as pseudo capacitor in energy storage applications[7,8,9].

In the last years, new spectroscopic methods, such as sum frequency generation[10,11] and sophisticated ab-initio molecular dynamics simulations[12,13] have shown that the behavior of the

double layer is not purely driven by electrostatics but it is often dominated by formation of chemical bonds and van der Waals interactions, by the free energy of solvation of interfacial species and, for water, by the formation of a so called bound interfacial layer[14]. Therefore, the nature of the electrical double layer, and hence the solid/liquid interface, can be influenced by both the nature and the concentration of dissolved species[14].

In electrocatalysis the best studied examples of such influences on the electrical double layer are the so-called cation effects[15]. By exchanging the cation, typically within the group of alkali metals, while maintaining all other experimental properties, researchers could modify the overpotential and the selectivity of catalytic reactions such as the CO_2 reduction reaction (CO_2-RR)[16], and the hydrogen evolution reaction (HER)[17]. Different reasons have been proposed for these effects that can be categorized in three main groups: First, the co-catalyst effect, where the presence of cations in the solution or adsorbed on the catalyst, can stabilize transition states of the catalysis process[18]. Second, field driven effects, where different sizes and solvation states of cations at the interface lead to a variety of length scales in the first electrolyte layer and therefore induce strong changes in the potential drop[19]. Strong electric fields can promote adsorption, stabilize charged transition states, or lead to the retention of competing electrochemical species[20]. Third, the presence of the cations influences the microenvironment at the solid liquid interface by either breaking the structure of bound interfacial solvents, change the pH at the interface, or lead to a phase separation at the electrode[21].These effects can influence mass transport, the free energy of solvation, and also stabilize transition states[22].

Exceptionally, in most of these studies the cesium cation exhibits by far the strongest influence on the observed catalytic reaction, as it leads to a highly increased turnover number for CO_2-RR and selectivity to higher C products on Cu catalyst[23], while boosting HER on gold catalysts[17]. This Cs behavior has been ascribed to its hydrophobic nature[24], small hydrodynamic radius[25], and its “soft” cloud of positive charge[26]. Despite numerous publications on cesium and of similar ions, crucial information, like concentration at the interface, solvation state, and its influence on the interfacial water layer, is sparse and mostly of theoretical nature.

In the present work we present an *in-situ* spectroscopic study of these effects, using interface-sensitive X-ray photoelectron spectroscopy (XPS), at a photon energy of 1000 eV, to determine the concentration of cesium ions within the first few nanometers adjacent to a suspended graphene electrode that acts also as a membrane that closes a flow cell. In the experiment we vary the cesium sulfate concentration in the electrolyte solution under open circuit potential (OCV). The XPS data are analyzed using the SESSA simulation package[27]. We also use X-ray absorption spectroscopy (XAS), to confirm the depletion of sulfate at the interfacial layer and its concentration dependence between interface and bulk regions. Lastly, using electrochemical impedance spectroscopy (EIS) we verify the high interfacial capacity due to excess concentration cesium ions at the interface. Ex-situ TEM, Raman, SEM and XPS were utilized after the experiments to assess the potential formation of graphene oxide, intercalation of cesium, and delamination of the graphene.

We observed an extraordinary behavior of Cesium ions in the EDL that can provide an explanation to the influence of cesium on electrocatalysis. Furthermore, it provides a guideline for the choice of electrolyte bulk concentration to reach maximum efficiency. We found that the interfacial behavior changes dramatically for Cs concentrations between 120 and 200 mM in aqueous solutions. This phenomenon opens new prospects to tailor interfacial parameters such

as hydrophilicity, pH, and potential gradient, with only minor changes to the system. Our study can inspire a new generation of electrolyte-driven techniques to control interfacial properties in electrocatalytic, energy storage and colloid chemistry applications.

Results

Methods

In-situ XPS experiments were performed in a custom-built electrochemical flow cell at the ambient pressure XPS endstation at beamline 11.0.2 of the Advanced Light Source (ALS) in Berkeley. The flow cell is sealed by a 200 nm thick Si_3N_4 holey membrane, fabricated with a rectangular array of circular holes of 485 nm diameter, spaced by 1300 nm, leading to a total open area of ~11 %. The Si_3N_4 membrane is covered with a 10 nm gold film to ensure electrical conductivity and it is sealed with three layers of graphene transferred individually onto the holy membranes utilizing the established direct wet transfer (see Figure 1). The graphene film closes the channels and is impermeable to liquids, but transmissive for electrons of relatively low kinetic energy. The graphene membranes can withstand pressure differences of several bar, as shown by Weatherup et al. and Yi Hsien et al.[28,29]

A Pt wire from Goodfellow and a leakless miniatureAg/AgCl from Mengel Engineering were utilized as a counter and reference electrodes, respectively. The flow cell volume is around 250 µl and can be operated at a flow rate of 1.5 ml/min in the vacuum environment (~$1x10^{-6}$ Torr) of the AP-XPS chamber, leading to a fully refreshed solution every 10 seconds. A Cs_2SO_4 stock solution of 200 mM concentration was injected and diluted with deionized water to create the reported concentration series. Pump-derived bulk concentrations, electrochemical sensitivity of the flow cell, and reference potential and impedance measurements were calibrated utilizing the redox ferricyanide pair utilized as internal standard in aqueous electrochemistry (for additional information on the flow cell and the calibration procedure see SI I).

Electrochemical impedance spectroscopy measurements were performed utilizing the same graphene window, flow cell setup, and similar electrolyte conditions, as in the XPS measurements, but with the cell outside the vacuum chamber.

XAS data were collected at beamline B07 of the Diamond Light Source in Oxford, UK, using an in-house electrochemical flow cell, with a Pt wire counter electrode and AgCl coated Ag wire reference electrode. The cell X-ray transmissive window was similar to that in the ALS experiments, but without holes and similarly covered 10 nm thick gold with 3 layers of graphene on top. TEM, Raman, XPS, SEM and electrochemistry were utilized after the XPS experiments to verify the presence of three layers of graphene, with an estimated 0.033 nm^{-2} density of defects, such as sp3 carbon, C-OH and C=O groups. The results indicate the absence of significant amounts of contamination (see SI II).

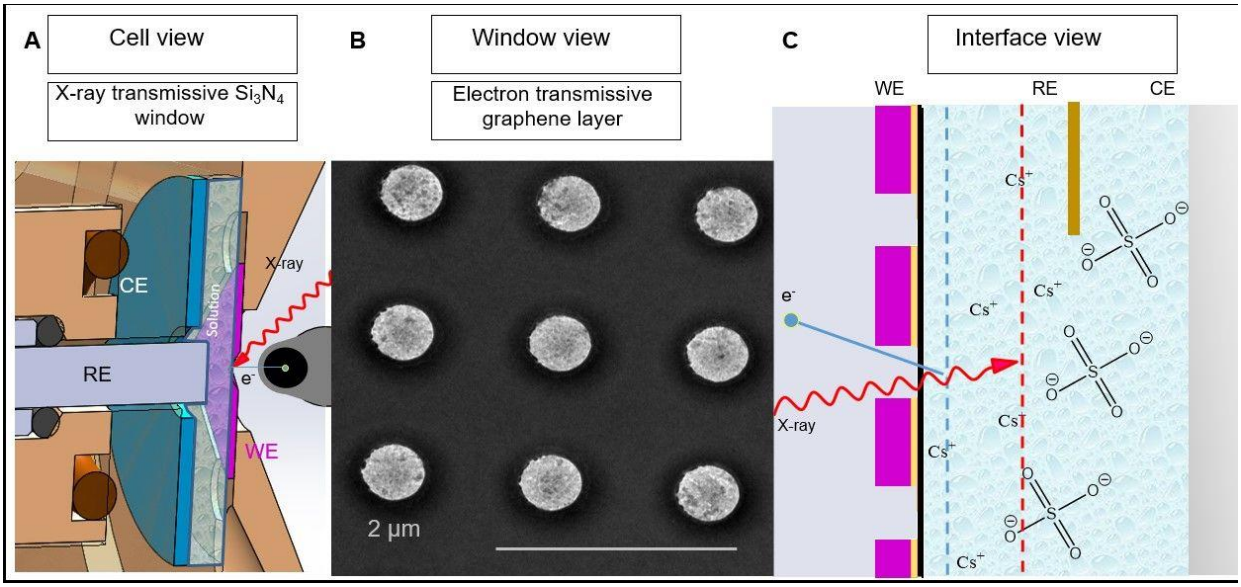

*Figure 1: Schematic of the sample geometry. **A**, left): Electrochemical flow cell featuring a Pt counter electrode, a Ag/AgCl reference electrode and an X-ray transmissive graphene-covered Si_3N_4 membrane as working electrode. The liquid volume is around 500 ul. X-rays from the 11.0.2 beamline at the advanced light source with an energy of 1000 eV illuminate the working electrode, in the high vacuum chamber, with a 55º degree incidence angle. **B**, center): TEM image of the region of interest in the 200 nm thick Si3N4 membrane, with 500 nm wide holes covered with a triple layer of graphene. The ratio between suspended graphene (over the holes) and graphene supported on a 10 nm Au layer is 1 to 9. **C**, right) Schematic of the X-ray and electron transmissive working electrode, based on the holey Si_3N_4 membrane (purple) covered with 2.5 nm Cr and 10 nm Au (yellow) to ensure good in-plane conductivity. The open holes and the gold coated parts are covered with a triple layer of graphene (thick black line). Aqueous solutions of Cs_2SO_4 of different concentrations flow through cell after introduction via capillary tubes.*

Interfacial cesium signal vs bulk concentration

Operando experiments were conducted in the three-electrode flow cell described above (Fig.1). During measurements, the sample was left at open circuit potential (OCP) and the working electrode was grounded. The OCP, measured against the Ag/AgCl reference electrode, was 0.225 $V_{Ag/AgCl}$. Interfacial Cs 4d photoemission spectra acquired as a function of Cs_2SO_4 concentration, from pure water to 200 mM, are shown in Figure 2A. The term interfacial will be used in the following to refer to information gathered for the Cs 4d peaks at kinetic energies of 920 to 935 eV, which have mean free paths of around 3.5 nm in water[30]. A plot of the Cs 4d peak areas vs bulk concentration is shown in Figure 2B. For concentrations up to ~100 mM, the interfacial cesium signal increases in a Langmuir-type fashion (see fit in Figure 2B). In a linear regression of the isotherm, the slope is 0.78 and deviates from the slope 1 expected for Langmuir isotherms. The lower slope indicates attractive behavior of Cs^+ ions towards the graphene surface.[31] The increase of peak intensity of interfacial Cs^+ is accompanied by a decrease in binding energy of 0.05 eV and an increase in peak width of ~1eV between 20 and 120 mM.

Unexpectedly, at 200 mM Cs_2SO_4 bulk concentration the Cs signal drops below the value measured at 40 mM. Since the signal intensity of reference C 1s and Au 4f XPS peaks did not change, the drop of the cesium signal is not accidental and can only be explained by a decrease in interfacial Cs^+ concentration, indicative of an intrinsic interaction between the Cs_2SO_4 electrolyte and graphene. Such extraordinary behavior of interfacial cesium ions when the bulk concentration increases above 120 mM is accompanied by a reversal of the trends in binding

energy and peak width changes: the first increasing by 0.13 eV from around 100 mM to 200 mM, and the width increasing from ~1.8 to 2.2 eV (Figure 2D).

The measured intenisty profile and the shift in binding energies[32] of the Cs 4d electrons can be explained by the adsorption of Cs^+ ions at the interface, as suggested earlier from the Langmuir isotherm fitting. Since the graphene electrode is grounded, we can use the binding energy of adsorbed cesium as our zero-shift reference. At 20 mM concentration, the interfacial signal is fully dominated by adsorbed cesium, hence displaying nominally minimal BE shift and minimal FWHM. At higher bulk concentrations, an increasing signal from fully solvated Cs cations shifted Cs doublet to lower binding energies due to the negative potential drop at the interface. The electrostatic gradient across the double layer potential drop then leads to the increases of full width half maximum (FWHM) with increasing Cs_2SO_4 concentration, as Cs species with different electrostatic contributions influence the measured spectra. (see Figure 2 D).

Apart from the dramatic decrease of the intensity, the FWHM data also show a deviation from the broadening trend as the values jump from 2.0 to 2.2 eV between 120 and 200 mM. This implies a correlation between the sudden decrease of cesium concentration at the interface and its change in electrostatic behavior. Displacement of Cs^+ by SO_4^{2-} and formation of Ion pairs between cesium and sulfate ions is the most likely explanation for all three observed phenomena (sudden decrease in intensity, decrease in BE and increase in FWHM of Cs 4d doublet), as caused by decrease of the interfacial Cs^+ concentration by replacement of adsorbed Cs^+ by sulfates. The ion pairs of Cs^+ and SO_4^{2-} ions share a solvation shell, decreasing the formal charge of the cluster[33,34] This leads to a decrease of the iterfacial e-field and therefore halts accelation of kinetic electrons that escape the electrolyte, leading to an apparent increased binding energy.

Baldelli et al[35]. observed such clustering of cesium and sulfate and consequential decrease of the induced electric field at the air-water interface utilizing sum frequency generation at high Cs_2SO_4 bulk concentrations of 3 M. To verify if the interfacial concentration of cesium at the electrolyte/graphene interface is sufficiently high to facilitate ion pairing and to validate the assumed Cs ion adsorption, we used the photoelectron spectroscopy simulation package SESSA (Simulation of Electron Spectra for Surface Analysis) to quantify the amount of cesium ions at the interface.

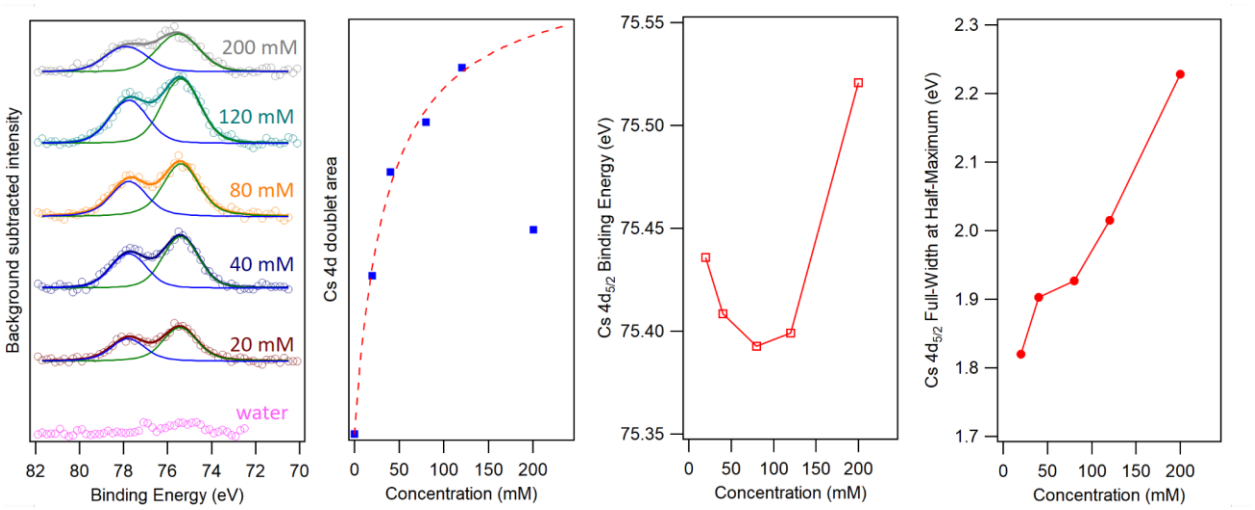

Figure 2: In-situ XPS measurements of cesium ions adjacent to the suspended graphene electrode as a function of Cs_2SO_4 bulk concentration. ***A*** *Recorded Cs 4d spectra of DI water and Cs_2SO_4 solution of different concentrations. Spectra are fitted with a Voigt doublet, branching ratio and spin-orbit splitting are fixed at 1.5 and 2.36 eV, respectively.* ***B*** *Concentration dependent intensity of the interfacial Cs 4d signal (blue squares). The increase in intensity between 20 mM and 120 mM Cs2SO4 bulk concentration can be expressed by the Langmuir isotherm (red dotted line). Drop in Cs intensity at 200 mM Cs_2SO_4 concentration contradicts established models.* ***C*** *Shift in Cs $4d_{5/2}$ binding energy with Cs_2SO_4 bulk concentration.* ***D*** *Full-width half-maximum of the Cs 4d signal as a function of bulk concentration.*

Measuring interfacial concentrations

To determine the amount of interfacial Cesium ions, the experimental spectra were simulated using peak fits from the SESSA package, photoemission, and Monte Carlo electron trajectory modeling software. The simulation process accounts for the sample and experimental geometry, the photoionization cross-sections, and the attenuation of photoelectron intensity due to depth of origin.[36,37] The ratio between Cs 4d and Si 2p (Si 2s) XPS signals from the substrate material was used for a comparison between the simulated and experimental spectra, to minimize effects of the analyzer transmission function, which we assumed to be constant within a narrow energy range of ~25 eV. The C 1s and O 1s XPS peak intensities were used as references to assess any attenuation of the signal due to the accumulation of adventitious carbon (see SI IV for the calibration of the SESSA model). Here C 1s originates from the measured graphene and carbon contaminations, O 1s is dominated by an interfacial layer of SiO_2 in the Si_3N_4 membranes and includes minor contributions from H2O, Hydrocarbons and oxidated defects in graphene.

The graphene triple-layer electrode and the subsequent attenuation of Cs 4d signal were simulated by a carbon layer of 1.3 nm thick, as reported for individually transferred 3 layers of graphene by Zhou et al.[38] caused by grain boundaries and wrinkles, which are lying flat due to our high-vacuum annealing above 200ºC[39]. The graphene thickness was calibrated using ex-situ XPS data collected from the graphene window rotated by 180 degree to monitor the attenuation of substrate signals by the layer (see SI V for more information).

Since the experiment uses a single photon excitation energy, the depth information from the Cs 4d intensity requires using a depth distribution model. Three models that capture the main outcome of our measurements are: a bulk model (constant concentration vs depth), a slice model (gradual decrease in concentration), and an adsorption model (step-like drop in concentration), as shown in Figure 3 A, B and C, respectively.

In the bulk model, we assume a constant bulk concentration throughout the EDL all the way to the interface (see Figure 3B). As depicted in Figure 3D? and Table 1, the simulated intensities at the experimental concentration for this model are an order of magnitude smaller than the measured intensities (0.02 vs. 0.26 at 40 mM) and the effect is more pronounced towards lower concentrations. In other words, the bulk concentration in the model matching the experimental data would have to be an order of magnitude larger than actual values. According to the widely accepted Gouy-Chapman Stern model[2], such increased ion concentration due to electrostatic interactions with the electrode, can only be found within the first few electrolyte layers (up to 1.3 nm), as the Debye screening length is below 1.3 nm under the experimental conditions. Therefore, another model with strong surface enrichment is needed to explain the measured data.

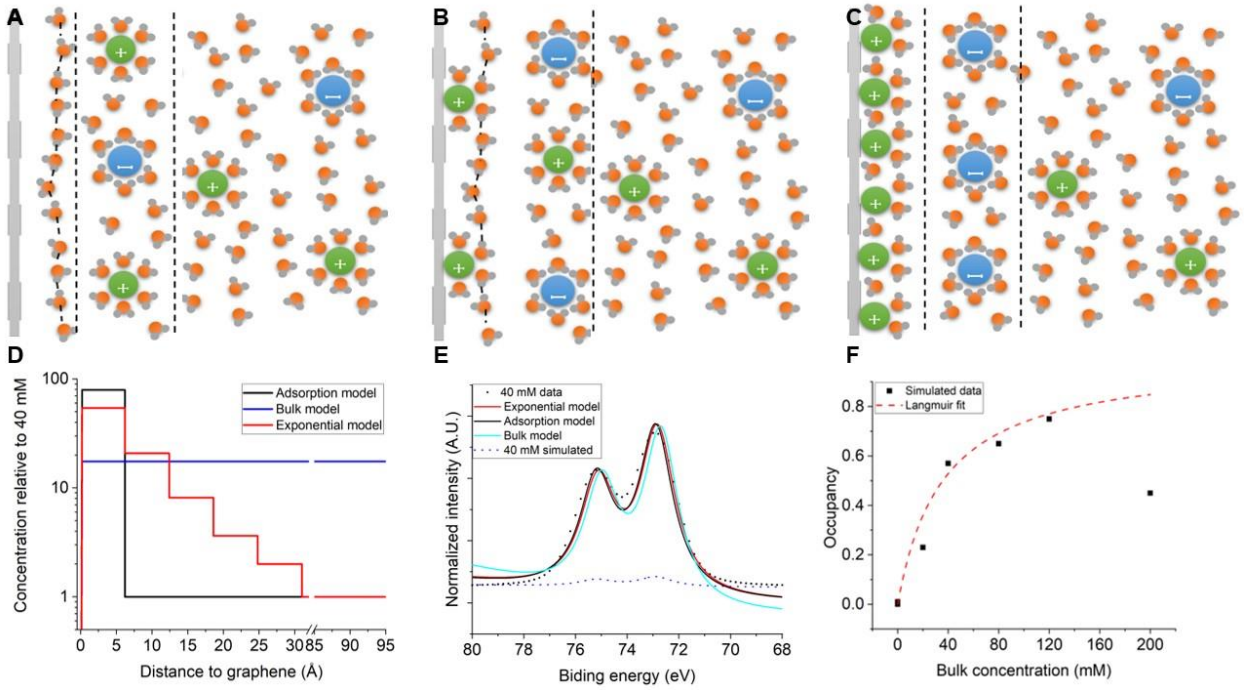

Figure 3: Assumed interfacial structure for three different concentration profile simulations, the gray bar represents suspended graphene, green spheres represent positively charged Cs^+ cations, blue spheres represent twice negatively charged sulfate anions, the water molecules from the solvent are represented in orange (oxygen) and gray (hydrogen). Black bars represent the separation between inner and outer Helmholtz layer. ***A*** *Bulk representation, no Cs^+ is adsorbed to the graphene, Cs^+ and SO_4^{2-} concentration is constant over the solution.* ***B*** *Sliced representation, Cs^+ ions are adsorbed in the inner Helmholtz plane, Cs^+ concentration is exponentially reduced with increasing distance to the electrode, reaching bulk concentration between 3 and 5 nm into the electrolyte.* ***C*** *Adsorption layer model, the electrode is fully covered by partly solvated Cs^+ ions, corresponding to an occupancy of 1 followed by a depletion layer and a direct transition to bulk concentrations after the first two layers.* ***D*** *Concentration profiles of the three different models with respect to the bulk concentration in dependence of distance to the electrode.* ***E*** *Comparison between simulated Cs 4d peak intensities of the adsorption model (black) the slice model (red) and the bulk model (cyan) to the experimental data (black squares) at 40 mM Cs_2SO_4 concentration and a simulated concentration of 40 mM Cs_2SO_4 (gray dotted line).* ***F*** *Estimated occupancy of a unit cell with a radius of 0.62 nm at the graphene/electrolyte interface in dependence of nominal concentration (black squares). Occupancies between 20 and 120 mM follow an extended Langmuir adsorption model (red dotted line). Occupancy at 200 mM drops to 50 % of the estimated Langmuir maximum.*

The adsorption model is constructed from a densely packed hexagonal 2D lattice of adsorbed cesium at the interface and a constant background concentration (see Figure 3 A left

schematic and Figure 3 E black curve), effectively creating a step-function concentration drop. Adsorbed cesium is assumed to shed half of the solvation shell it had in the bulk, so that each cesium atom is left with four [40] water molecules. The equivalent Cs_2SO_4 bulk concentration with the same water-to-cesium ratio is 4.5 M.

The Cs–O–Cs distance in the hexagonal lattice is twice the Cs–O distance in bulk solutions (3.07Å)[40] and the thickness of the layer was estimated as the sum of the Cs–O distance and the radii of Cs^+ (1.7 Å)[40] and water (1.7 Å), or 6.47 Å in total. Partial occupation of this layer was calculated by filling the vacancies with background concentration, i.e. statistical occupation as in the bulk. The Cs coverage θ (a number between 0 and 1) fitted to the experimental intensity is given in Table 1. It ranges from a coverage of 0.2 at 20 mM to 0.75 at 120 mM, with an area per unit charge of 160 and 41 $Å^2$/e, respectively (see Figure 3 F). At full occupation the model gives a relative intensity of Cs 4d to Si signal equal to 1.0%.

The slice model (Figure 3B. Figure 3 E and D red curves) serves as a comparison between adsorption and bulk model. It mimics a Gouy-Chapman-like exponential decrease of the Cs^+ concentration with a slice thickness of twice the Cs-O distance in bulk solutions. Comparison of the slice and adsorption layer model show that the interfacial Cs signal is dominated by the first densely packed layer, leading to a maximum decrease in occupancy by only 18 % when utilizing the different models. Therefore, the slice model effectively converges to the adsorption model and the claim of a Cs^+ interfacial layer enriched by at least 30 times the bulk concentration is valid under all simulated conditions. Further elucidating on this enrichment, the highest difference between simulated Cs4d intensity and measured interfacial intensity is found for 40 mM Cs2SO4 bulk concentration. Utilizing the three different models fitted to the measured data, a coverage of 0.57 is reached for the adsorption model and a coverage of 0.39 for the exponential mode. The above defined unit cell was used to calculate molarity and density of these adsorbed first 0.614 nm of electrolyte. At intensities fitted to 40 mM data, this first layer exhibits a Cs+ concentration of 6.4 M for the adsorption model (see Table 1), of 4.3 M for the slice model and 1.4 M for the bulk model. This equals excess concentrations of 80, 54 and 18 times the expected 80 mM Cs+ bulk concentration (Figure 3 D). Similar to the interfacial Cs^+ intensity, the estimated occupancy drops by about 30 % when the bulk concentration is increased from 120 mM to 200 mM.

Table 1: Results from experiments and the SESSA bulk and adsorption model simulations; for the bulk model the simulated Cs 4d / (Si 2s + 2p) intensity ratios (I_{Cs} / I_{Si}) are given for the experimental concentrations (c_{exp}), and the model concentrations (c_{mod}) at the experimental intensity ratios (I_{exp}) are given next to it; the scaling factors to the respective experimental values are given in brackets; for the adsorption model the occupancy (θ_{mod}) at experimental intensity ratios (I_{exp}) are given next to the respective area per charge.

c_{exp}	$I_{exp} = I_{Cs} / I_{Si}$	θ_{mod} fit to I_{exp}	c(Cs+) adsorbed layer	area / charge
Experimental		**Adsorption model**		
mM	%		M	$Å^2$ / e
20	0.26	0.22	2.6	141
40	0.61	0.57	6.4	57
80	0.71	0.65	7.3	50
120	0.84	0.75	8.4	43
200	0.58	0.45	5.2	72

Based on quantitative analysis of the XPS measurements, the enhancement in interfacial cesium concentrations creates suitable conditions for the appearance of ion-pairing. To confirm these findings, we employed interface and bulk sensitive XAS measurements to investigate the role of sulfate during the decrease of interfacial Cs^+ signal.

Depletion of interfacial cesium and accumulation of interfacial sulfate at 200 mM

A liquid cell with a working electrode made of three layers of graphene (TLG) was used for X-ray absorption spectroscopy of the sulfate anions at 40, 120, and 200 mM concentrations. The fluorescent yield (FY) and electron yield (EY) [41–43] cesium M edge and sulfur K-edge are shown in figure 4. The two signals have very different probing depths. While FY stems largely from the first 30 µm (the attenuation length at the edge in ice),[44] the EY has a probing depth estimated to be below one nanometer[41]. As expected, the bulk sensitive FY signal scales linearly with concentration for both sulfate anions and cesium cations (see Figure 4 A and C). In stark contrast, the EY signal intensity, which is nonlinear for both. While the XPS peak intensities decrease change by a factor of 1.5, the interfacial Cs M edge white-line intensity decreases by a factor of 0.77 (instead of the 1.5x increase observed in bulk) between concentrations of 120 and 200 mM (see Figure 4 B). In contrast, when increasing the Cs_2SO_4 concentration from 120 to 200 mM, the white-line intensity of the sulfur K-edge increases by a factor of 2.5 (instead of 1.7, as expected from the increase in bulk concentration). This suggests that the decreased concentration of cesium is accompanied by an increase in interfacial sulfate concentration, which strongly implies an interface specific ion pairing. The overall reduced intensity of the interfacial sulfur K-edge signal can be attributed to several factors. First, the flux of photons, which is proportional to the upstream drain current in the Kirkpatrick-Baez mirrors (I0) of the B07 beamline in the diamond light source, is more than an order of magnitude smaller at 2465 eV than at 738 eV. Second the absorption cross section of the S K-edge is 43 times smaller than Cs M edge and the concentration of sulfate is half the concentration of cesium [45.] Together with the decay of photoelectric relaxation with higher photon energies, this leads to a strongly reduced amount of photoionization of sulfate K-edge close to the interface compared to that in Cs. The high signal to noise ratio of the FY K-edge signal can be assigned to the strongly increased probing volume. Kinetic electrons with 2465 eV exhibit an inelastic mean free path in

water that is about 7.5 nm, which is 2.6 times higher than at 738 eV for the Cs M-edge[30] and thus generate many more secondary electrons. Additionally, a major contribution of the TEY signal is generated by Auger and secondary electron emission, with kinetic energies that do not scale with incident photon energy, effectively reducing the difference in probing dept further. In comparison the attenuation length of photons at 2465 eV in water is 12.1 times higher than for photons at 1000 eV[46]. Lastly, under the assumption of a sub nanometer probing depth, proposed by Velasco Velez et al.[41] and further demonstrated by van Spronsen et al,[43], the small electron yield response of the sulfur K-edge suggests that the ion clusters formed from Cs^+ and SO_4^{2-} are not directly adsorbed on graphene and therefore their signal is more attenuated.

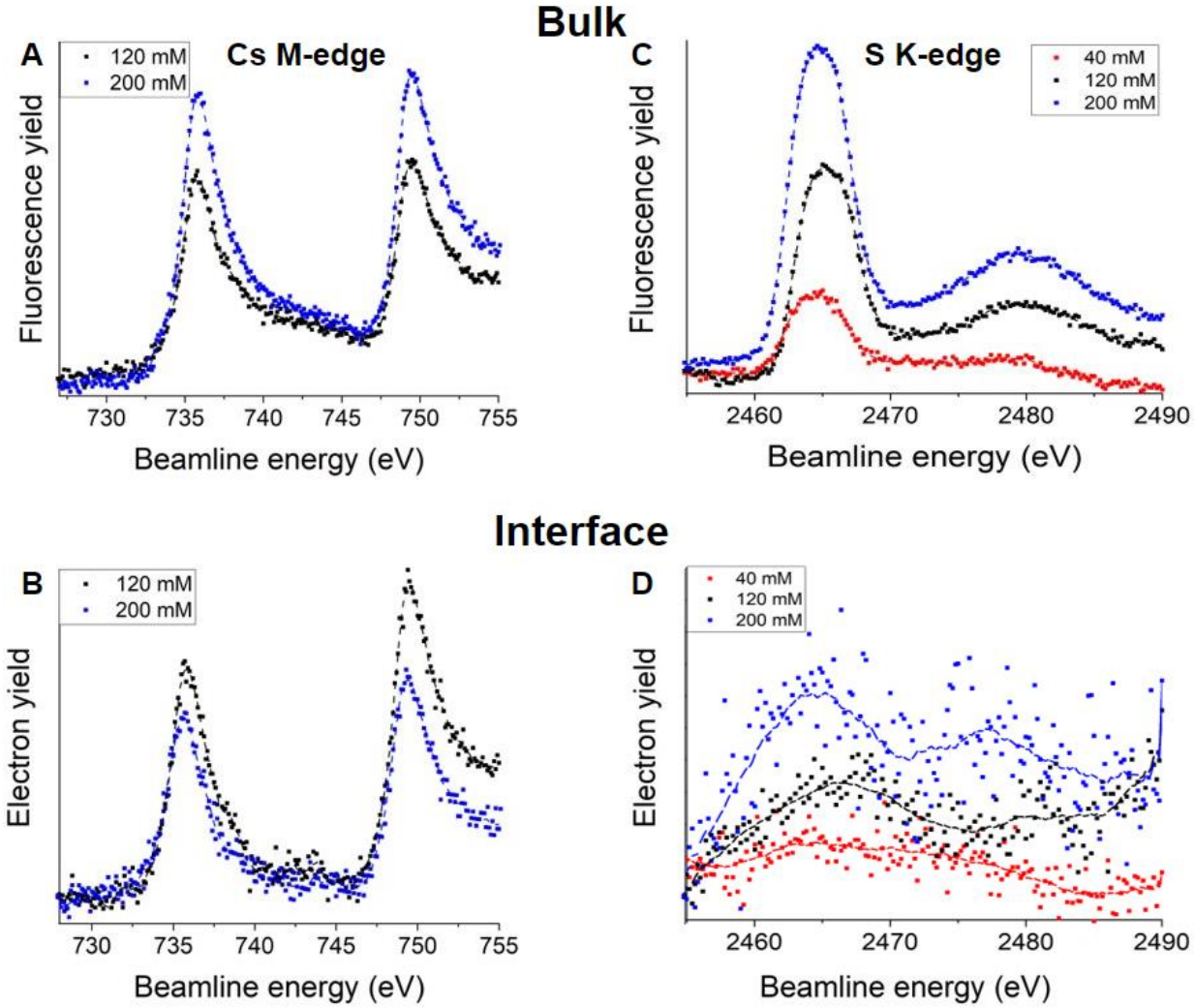

Figure 4: XAS at the graphene/electrolyte interface in an electrochemical flow cell. No potential control applied, OCV was 0.225 V vs. Ag/AgCl. Cs_2SO_4 concentration dependent bulk sensitive fluorescence yield spectra of the Cs M edge (A) and S K-edge (C) probe around 30 µm deep into the solution and show a linear increase in intensity. Interface sensitive electron yield spectra of the Cs M edge (B) and S K-edge (D) collected through drain current at the working electrode probe the first few nm adjacent to the electrode and show a decrease in Cs signal accompanied by a significant increase in S signal between 120 and 200 mM bulk concentration.

The spectral shape of both the Cs M-edge and the sulfur K-edge in the bulk sensitive fluorescence measurements for 120 mM and 200 mM shows no dissimilarities suggesting no

detectable ion pairing within the bulk electrolyte. The interfacial Cs M-edge shows a slight broadening of the peak which might be indicative of the changed electronic environment as the cesium ions form pairs with sulfate in the electrical double layer. Unfortunately, the interfacial S K-edge data is too noisy for any shape related interpretation.

It is worth noting that, as explained before, the XAS measurements were conducted on a fully continuous gold film, therefore the observed excess cesium concentration is not exclusive to suspended triple layers of graphene.

As spectroscopic data from both techniques suggest an adsorbed cesium layer, electrochemical impedance spectroscopy was utilized to understand whether the formation of this layer is accompanied by partial charge transfer.

Electrochemical characterization of the Cs^+/graphene double layer

To assess the likelihood of Cs adsorption, the electrode capacitance and electrical resistance against Faradaic processes was measured using electrochemical impedance spectroscopy (EIS). A potential variation of ±5 mV and decreasing frequencies from 50 kHz to 50 mHz were used during the measurements. EIS was performed on the TLG-Pt with the cell exterior held under ambient conditions to minimize the pressure difference across the SiNx membrane and consequential stress, reducing the possibility of leakage. Impedance data of 120 mM and 200 mM Cs_2SO_4 bulk concentrations are shown in the Bode (Figure 6 A) and the Nyquist (Figure 6B) representation.

The Bode plot at 120 mM exhibits a low impedance at high frequencies, rapidly rises at intermediate frequencies, and levels out at low frequencies. This behavior is representative for bulk concentrations of 40, 80, 120 and 160 mM (shown in Figure SI V) and is indicative of Faradaic and non-Faradaic contributions. Similarly, the Nyquist plot (Figure 6B) consists of one dominant semicircle, characteristic of one process dominating cell impedance. Our results contrast with literature reports on graphene and graphene oxide samples that used typical supporting electrolyte solutions, which report a closing semicircle on lower frequencies, indicating a non-capacitive process.[38] These non-capacitive currents can be caused by Faradaic processes, such as a redox process or by the modification of the electrode excess charge, due to adsorption, intercalation or chemical modifications of graphene.[40] Non cesium related Faradaic processes and graphene modifications can be assumed to be negligible, as polished Pt electrodes exhibit a blocking electrode behavior in the same setup and under the same conditions (see SI V for more information). Comparable EIS with KCl did not exhibit Faradaic behavior on comparable graphene electrodes as reported by Bonanni et al.[47] and Angizi et al.[48], implying that the observed effects (per Figs. 6A and 6B) are indeed specific to Cs ions and suspended graphene electrodes.

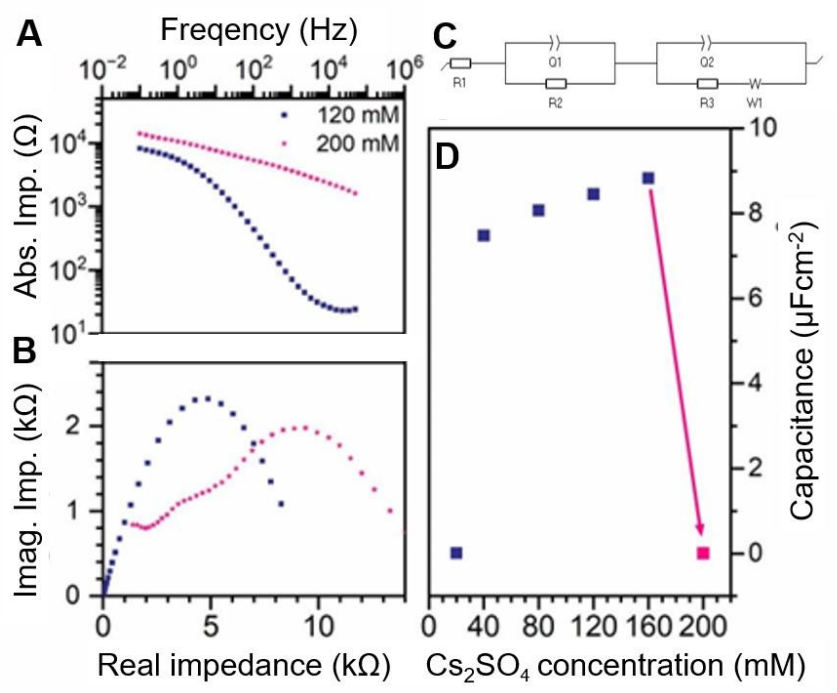

Figure 5: Electrochemical impedance measurements on the TLG sample at different bulk concentrations of Cs_2SO_4 at open circuit potential and under static conditions. Voltage modulation is 5 mV, shown data are averaged over two consecutive scans. ***A*** *Bode representation of the obtained data for 120 (blue) and 200 (purple) mM Cs2SO4 bulk concentrations.* ***B*** *Nyquist representation of the data shown in A.* ***C*** *Estimated capacity of the first high frequency circuit, corrected for electrode area, versus Cs bulk concentrations.*

At 200 mM Cs_2SO_4, the Bode plot shows resistive behavior with nearly linearly increasing impedance towards lower frequencies and the Nyquist plot shows a second smaller semicircle between 2 and 5 kΩ. Both changes suggest a transition from linear diffusion to a partly covered and inactive electrode.[49,50]

To compare several measurements quantitatively, we will focus on the changes in double layer capacity with electrolyte concentration. The double layer is represented together with other resistive and capacitive elements in the cell by an extended Randles equivalent circuit model (R_1-(Q_1,R_2)-(Q_2,R_3-W_1)), as depicted in Figure 5C. The equivalent circuit is used to deconvolute the overall permittivity into the bulk resistance of the cell (R_1), the resistance and capacitance of the electric double layer (Q_1&R_2) and a circuit model typically used for porous electrode materials with intercalating ions, such as in Lithium-ion batteries (Q_2, R_3 & W_1).[51] The effective double layer capacitance C_{eff} is calculated using equation 1 from the respective constant phase element parameters. Y and R_P represent the measured capacitance and the charge transfer resistance, respectively, and n is the exponential factor of the constant phase element:

$$C_{eff} = \frac{(Q_1 R_P)^{\left(\frac{1}{(n)}\right)}}{R_p} \sin\left(\frac{n\pi}{2}\right) \qquad \text{Eq.1}$$

Fitting the effective capacitance of the double layer for all concentrations shows significant variations for 20 and 200 mM Cs_2SO_4 in comparison with the almost linear dependency for other measured concentrations (see Figure 5D). This indicates a breakdown of the assumed model and a dramatic change in electrode/electrolyte behavior under these conditions. The trend of an increasing amount of charge carriers on the electrode with increasing Cs^+ bulk concentration is broken between 160 mM and 200 mM. Therefore, our EIS data suggest in accordance with the spectroscopic results that between 20 and 160 mM bulk Cs_2SO_4 concentrations, Cs^+ ions adsorb at the graphene surface, leading to a partial electron transfer. For higher concentrations, the model loses its validity, corroborating ion pairing as evidenced by spectroscopy.

Discussion

The quantitative analysis of *in-situ* XPS and XAS data suggests an accumulation of cesium ions within the first electrolyte layer by more than a factor of 60 compared to the bulk concentration. Furthermore, we observe a stronger Cs accumulation at lower bulk concentrations, leading to a Langmuir isotherm-like[31] concentration dependence of the measured Cs signal. Another evidence of this behavior are the observed changes in electronic structure, most likely due to a change in solvation state, as the cesium ions adsorb on the graphene surface. This assumption is supported by the BE shifts and FWHM of the interfacial Cs 4d XPS signal (see section II), the narrowing of Cs M-edge (see section IV) spectra, and the high capacity of the electrochemical system (see section V).

From an electrostatic point of view, the adsorption-based model is also the most appropriate to explain the measured interfacial Cs signal intensity, as it poses the lowest possible overcharging. A Cs ion closer to the electrode gives rise to a larger XPS signal, so a model reaching further into the bulk needs a larger ion excess for the same intensity. The excess charge estimated using the adsorption model at 120 mM is ~35 $\mu C/cm^2$, while the bulk model yields 109 $\mu C/cm^2$ excess charge. The charge expected from EIS is, at maximum, 10 $\mu C/cm^2$, so both models would overcharge, leading to a reduced entropic cost for the adsorption model.

In fact, cesium ions exhibit several properties that render a deviation from the Gouy-Chapman model to a chemically driven adsorption likely. First, cesium does not fit into the dominant double layer models that are based on the Poisson-Boltzman distributions, which assume point-like, nonpolarizable charges that are non-correlated. Effects of solvation are also not considered. For Cs ions, these assumptions are incorrect. Cs ions have with 3.4 Å a large ion diameter [41] that is highly polarizable, due to extended π-Orbitals, a property that has been shown to lead to stronger adsorption on graphite-like materials.[52,53] Simultaneously, Cs ions are structure-breaking (lead to fewer hydrogen bonds), which causes a smaller hydration shell than that of Li or Na ions.[54] Consequently, Cs ions and surrounding water molecules have a larger mobility than Li or Na,[53,54] leading to a more positive entropic contribution.

Secondly, cesium's hydrophobic nature leads to a decrease in free energy of solvation, when the solvating water molecules are released. Effects of this hydrophobicity leading to an excess of cesium ions around hydrophobic interfaces, as shown for ionic micelles by Joshi et al.[55], for a liquid/liquid phase separation by Schnell et al.[56]. Recently, Serva et al.[57] discussed the formation of hydrophobic water/water interactions in the first two electrolyte layers adjacent to hydrophobic surfaces. These interactions lead to the formation of hydrophobic cavities, effectively

reducing the free energy of solvation for hydrophilic ions close to such interfaces. In the case of the present work the highly hydrophobic water/graphene interface appears to form a huge hydrophilicity gap close to the electrode, for which the large cesium ions show a strong affinity.

Lastly, the high polarizability of both Cs and the graphene electrode leads to a partial charge transfer between the ion and the surface[47], which we detected in the Faradaic-like response during EIS measurements. This electron transfer leads to a decreased free energy of the graphene water interface and decreases the nominal charge of the adsorbed Cs layer, leading to a weakened electrostatic repulsion between solvated Cs+ and the electrode. Indeed, our molecular dynamic simulations show that the presence of adsorbed Cs with a nominal valency of 0.92 at the interface facilitates a higher Cs+ density close to the electrode, while the highest SO_4^{2-} density is observed at around 0.8 nm into the solution (see SI VI for molecular dynamics and DFT calculations). Additionally, to electrostatic and solvation effects, the presence of adsorbed Cs leads to the relaxation of the multilayer graphene structure in some of the simulated cases, further reducing the total free energy of the electrode system. In summary, all employed methods show a strong deviation for the observed interfacial behavior between bulk concentration of 120 and 200 mM of Cs_2SO_4 as the Cs signal both in XPS and XAS-EY dramatically decreases. Coupled with the rapid increase of interfacial sulfate between these concentrations and a strong decrease of measured capacity in EIS, we conclude that the solvation behavior of cesium and sulfate changes around these concentrations. This phenomenon can be credited to an ion pairing between cesium and sulfate that creates uncharged clusters at the interface. This is observable in the blocking electrode-like behavior of 200 mM EIS, the steep increase of Cs binding energy and the increase in sulfate concentration at the interface.

To explain these results, we compare the found interfacial layer to bulk concentrations with similar ionic strength, i.e. above 1 M. Literature reports from Lee et al and Gaddam et al. show that ions in such solution start to pair, effectively forming a charge neutral Cs_2SO_4 cluster in one single solvation shell.[58,59] Additionally, Baldelli et al. showed that the induced electric field formed at the electrolyte/air interface, due to asymmetric ion adsorption, is fully screened in 1.7 M Cs_2SO_4.[60] In contrast, H_2SO_4 electrolytes at the same concentration exhibit a strong electric field perpendicular to the interface. Similar effects were observed by Lee et al.[61] for the pairing of Cs+ with the surfactant dodecyl sulfate, leading to the intercalation of Cs into the polar micelle shell, forming layered shell structures. In contrast, similar micelles with Na^+ as cations exhibit a clear separation between micelle and counterions. This pairing of ions can provide an explanation for the observed changes. When sulfate anions are paired with Cs cations, they would adsorb together, blocking the electrode and react less to the charge on the electrode, in turn reducing capacitance and XPS signal enhancement/suppression with varying potentials. Consequently, the interfacial intensity of sulfur increases. The ions are not as densely packed as Cs ions alone and the interfacial Cs intensity is reduced. The ion pairing also reduces the effective ion concentration and hence increases the debye length[62,63].

Measurements in bulk solutions or solution-vacuum interfaces usually see ion pairing at or above 1 M concentrations, so the transition between 160 and 200 mM Cs_2SO_4 in our study is an interfacial effect. Therefore, ion pairing in low concentrated electrolyte solutions in electrochemical processes cannot be excluded. This effect allows subtle adjustments in bulk concentration to exert profound control over the electrical double layer properties, pH, and electrode hydrophilicity[64,65].

Conclusion

We examined the interface between suspended few-layer graphene electrodes and Cs_2SO_4 electrolytes using *in-situ* X-ray spectroscopies. Our approach allows us to quantitatively probe the first few nanometers adjacent to the electrode using both core photoelectrons (XPS) and secondary electron yield (XAS). To quantify the Cs ion excess at the interface, we compared measured intensities to interfacial models with the electron photoemission simulation package SESSA.

Two very distinctive EDL behaviors were observed for this system. For lower concentrations (interval of 20-120 mM), we determined that the interfacial Cs concentration within our probing depth of ~ 3 nm is at least 2.5 times the bulk concentration and at most 6.5 times the bulk concentration, depending on the utilized model. This surpasses the concentrations expected from the Gouy Chapman model for low-concentrated electrolytes and weakly polarized electrodes.

From the experimental data obtained in our measurements and models discussed, an adsorbed layer of cesium ions that partly shed their solvation shells describes our experimental evidence the best. The reasons are manifold. Firstly, the concentration-dependence of interfacial cesium follows Langmuir-type behavior. Secondly, the Cs 4d line shape (broadening/asymmetry) and binding energy evolution indicates that Cs ions reside in a narrow distribution of potentials. The third reason is that interface-sensitive S K-edge absorption spectroscopy of the SO_4^{2-} counterion shows that the excess of Cs ions in the double layer leads to a depletion of sulfate, as would be expected with an adsorbed layer of Cs ions. From the EIS results, we observed Faradaic-like behavior around the open circuit potential, indicating charge transfer between Cs ions and the graphene electrode. Lastly, the adsorption model minimizes overscreening by the ions, which was observed at all concentrations within 20-120 mM interval.

An important driver of Cs ion adsorption on graphene is its colloidal behavior, based on the following reasons. Firstly, the overscreening of the electrode potential, as elucidated in the discussion section is a sign of specific interaction with the electrode and the ions. Secondly, a linear regression of the measured adsorption isotherm is below one, which is associated with an attractive tendency of the adsorbate. Another reason is that the sulfate signal remains barely observable by the interface-sensitive XAS measurements at potentials up to 0.3 V above the expected point of zero. This indicates an overpotential for anion attraction caused by cation interactions other than field-dependent ion accumulations. We attribute the colloidal behavior to the high polarizability of cesium combined with a recessed image charge on graphene, entropic increase by release of solvating water molecules, and ionic bonding with terminating carboxylic groups at grain boundaries. However, our methods do not allow any discrimination between these effects.

The above adsorption model is no longer valid at 200 mM Cs_2SO_4, where we observed a very distinct EDL behavior: a strong increase of interfacial sulfur signal, a sharp drop of interfacial Cs concentration, and a sharp drop of double layer capacitance accompanied by blocking behavior of the electrode. We explain these observations by (interfacial) ion pairing, or ion

clustering: the presence of uncharged Cs_2SO_4 clusters serve as a vehicle for sulfate species to approach the interface and simultaneously reduce the density of interfacial Cs. Along similar lines, the energy of solvation of sulfate is larger than for Cs ions, leading to a better solvation of uncharged Cs_2SO_4 clusters. In turn, the tendency of Cs to accumulate at the interface is reduced. The clustering also lowers the effective charge carrier density, which is reflected in a reduced capacity to react to applied potentials. Interestingly, ion clustering to form uncharged solvated species behavior has not been observed in the bulk of 200 mM Cs_2SO_4 solutions[66], so we expect this effect to be strictly interfacial. From our quantitative measurements and modeling, we estimated the local interfacial concentrations of up to 2 M within the first nanometer. This points out once again the importance of interface-specific probes applied to real electrochemical systems.

Our findings hence indicate two distinct double layer behaviors on graphene, depending on the Cs_2SO_4 bulk concentration. Below 160 mM and below +0.3 V vs pzc, we find a Cs-dominated adsorption model, while above 160 mM, ion pairing can explain the experimental results. This means that there is a relatively narrow concentration window for the observation of strong cation-specific effects in electrocatalytic applications. And although the cation effect on graphene has not been studied to our knowledge, the strong dependence on bulk concentration might be the reason for large variations in reports on cation effects, for example in CO_2 reduction studies[67].

Acknowledgements

This work is funded by the Office of Basic Energy Sciences (BES), Chemical Sciences, Geosciences, and Biosciences Division, of the U.S. Department of Energy (DOE) under Contract DE-AC02-05CH11231, FWP CH030201 (Catalysis Research Program). L. J. F. acknowledges support from the Alexander von Humboldt Foundation, Bonn, Germany. XPS measurements and reference XAS measurements were conducted on beamlines 11.0.2, 9.3.2 and 9.0.1 of the Advanced Light Source, a U.S. DOE Office of Science User Facility under contract no. DE-AC02-05CH11231, the 23-ID-2 (IOS). Sample preparation and characterization by TEM, Raman, AFM, SEM and XPS were conducted at the Molecular Foundry, a U.S. DOE Office of Science User Facility under contract no. contract number DE-AC02-05CH11231. The authors want to thank Diamond Light Source for access on beamline B07 (SI35104) that contributed to the results presented here. This research used resources of the National Energy Research Scientific Computing Center (NERSC), a Department of Energy Office of Science User Facility using NERSC award <BES>-ERCAP<0030529> We want to thank Grolltex for providing the used graphene as samples for basic research purposes. We want to thank Oleg Costco from beamline 9.0.1 of the Advance Light Source for his help with setting up In-situ XAS measurements. We want to thank Hao Chen and Antoine Laine for fruitful discussions on sample setup and measurement procedure. We want to thank Ka Chon Ng, Lisa Schardt and Tanner Pearson for their support during liquid cell XPS experiments at beamline 11.0.2.

References

(1) Schmickler, Wolfgang; Santos, Elizabeth. *Interfacial Electrochemistry*, 2nd ed.; Springer Berlin Heidelberg: Berlin, Heidelberg, 2010. https://doi.org/10.1007/978-3-642-04937-8.

(2) Allen J. Bard and Larry R. Faulkner, Electrochemical Methods: Fundamentals and Applications, New York: Wiley, 2001, 2nd ed. https://doi.org/10.1023/A:1021637209564

(3) Jacob N. Israelachvilli, Intermolecular and Surface Forces, 3rd ed.: Amsterdam: Elsevier, 2011, https://doi.org/10.1016/C2011-0-05119-0

(4) Paul C. Hiemenz and Raj Rajagopalan, Principles of Colloid and Surface Chemistry, 3rd ed.: Marcel Dekker, New York,1997 , https://doi.org/10.1016/C2011-0-05119-0

(5) Sposito, G. (2016). Gouy-Chapman Theory. In: White, W. (eds) Encyclopedia of Geochemistry. Encyclopedia of Earth Sciences Series. Springer, Cham. https://doi.org/10.1007/978-3-319-39193-9_50-1

(6) Langmuir 2015, 31, 42, 11477–11483 Publication Date:October 16, 2015 https://doi.org/10.1021/acs.langmuir.5b02389

(7) Nørskov, J. K.; Rossmeisl, J.; Logadottir, A.; Lindqvist, L.; Kitchin, J. R.; Bligaard, T.; Jónsson, H. Origin of the Overpotential for Oxygen Reduction at a Fuel-Cell Cathode. *J. Phys. Chem. B* **2004**, *108* (46), 17886–17892. https://doi.org/10.1021/jp047349j.

(8) Rossmeisl, J.; Qu, Z. W.; Zhu, H.; Kroes, G. J.; Nørskov, J. K. Electrolysis of Water on Oxide Surfaces. *J. Electroanal. Chem.* **2007**, *607* (1–2), 83–89. https://doi.org/10.1016/j.jelechem.2006.11.008.

(9) Shi, Chuan; Hansen, Heine A.; Lausche, Adam C.; Nørskov, Jens K. Trends in Electrochemical CO2 Reduction Activity for Open and Close-Packed Metal Surfaces. *Phys. Chem. Chem. Phys.* **2014**, *16* (10), 4720–4727. https://doi.org/10.1039/c3cp54822h.

(10) Shanshan Yang, Xiao Zhao, Yi-Hsien Lu, Edward S. Barnard, Peidong Yang, Artem Baskin, John W. Lawson, David Prendergast, and Miquel Salmeron, Journal of the American Chemical Society 2022 144 (29), 13327-13333, DOI: 10.1021/jacs.2c03344

(11) Steffen Murke, Wanlin Chen, Simone Pezzotti, and Martina Havenith, Journal of the American Chemical Society 2024 146 (18), 12423-12430, DOI: 10.1021/jacs.3c13633

(12) Aashish Tuladhar, Shalaka Dewan, Simone Pezzotti, Flavio Siro Brigiano, Fabrizio Creazzo, Marie-Pierre Gaigeot, and Eric Borguet, Journal of the American Chemical Society 2020 142 (15), 6991-7000DOI: 10.1021/jacs.9b13273

(13) Sudarsan Surendralal, Mira Todorova, Michael W. Finnis, and Jörg Neugebauer, Phys. Rev. Lett. 120, 246801 – Published 12 June 2018

(14) Simone Pezzotti, Alessandra Serva, Federico Sebastiani, Flavio Siro Brigiano, Daria Ruth Galimberti, Louis Potier, Serena Alfarano, Gerhard Schwaab, Martina Havenith, and Marie-Pierre Gaigeot

The Journal of Physical Chemistry Letters 2021 12 (15), 3827-3836

DOI: 10.1021/acs.jpclett.1c00257

(15) Monteiro, M.C.O., Dattila, F., Hagedoorn, B. et al. Absence of CO2 electroreduction on copper, gold and silver electrodes without metal cations in solution. Nat Catal 4, 654–662 (2021). https://doi.org/10.1038/s41929-021-00655-5

(16) Monteiro, Mariana C. O.; Dattila, Federico; López, Núria; Koper, Marc T. M. The Role of Cation Acidity on the Competition between Hydrogen Evolution and CO2Reduction on Gold Electrodes. *J. Am. Chem. Soc.* **2022**, *144* (4), 1589–1602. https://doi.org/10.1021/jacs.1c10171.

(17) Monteiro, Mariana C. O.; Goyal, Akansha; Moerland, Pricilla; Koper, Marc T. M. Understanding Cation Trends for Hydrogen Evolution on Platinum and Gold Electrodes in Alkaline Media. *ACS Catal.* **2021**, *11* (23), 14328–14335. https://doi.org/10.1021/acscatal.1c04268.

(18) Zhang, Z., Li, H., Shao, Y. et al. Molecular understanding of the critical role of alkali metal cations in initiating CO2 electroreduction on Cu(100) surface. Nat Commun 15, 612 (2024). https://doi.org/10.1038/s41467-024-44896-x

(19) Jay T. Bender, Amanda S. Petersen, Frederik C. Østergaard, Mikayla A. Wood, Sean M. J. Heffernan, Delia J. Milliron, Jan Rossmeisl, and Joaquin Resasco, ACS Energy Letters 2023 8 (1), 657-665, DOI: 10.1021/acsenergylett.2c02500

(20) Marcus Theory: Thermodynamics CAN Control the Kinetics of Electron Transfer Reactions, Todd P. Silverstein, Journal of Chemical Education 2012 89 (9), 1159-1167, DOI: 10.1021/ed1007712

(21) S. R. Alfarano , S. Pezzotti , C. Stein , Z. Lin , F. Sebastiani , S. Funke , K. Mauelshagen , C. Hoberg , I. Kolling , C. Y. Ma , T. Ockelmann , G. Schwaab , L. Fu , J. B. Brubach , R. Pascale , M. Head-Gordon , M.-P. Gaigeot , K. Tschulik and M. Havenith , Stripping away ion hydration shells in electrical double-layer formation: Water networks matter, Proc. Natl. Acad. Sci. U. S. A., 2021, 118 , e2108568118

(22) B. Timmer , M. Sluyters-Rehbach and J. H. Sluyters , Electrode kinetics and double layer structure, Surf. Sci., 1969, 18 , 44 —61

(23) Elena Pérez-Gallent, Giulia Marcandalli, Marta Costa Figueiredo, Federico Calle-Vallejo, and Marc T. M. Koper, Journal of the American Chemical Society 2017 139 (45), 16412-16419, DOI: 10.1021/jacs.7b10142

(24) A Study of the Hydration of the Alkali Metal Ions in Aqueous Solution, Johan Mähler and Ingmar Persson, Inorganic Chemistry 2012 51 (1), 425-438, DOI: 10.1021/ic2018693

(25) Resasco, Joaquin; Chen, Leanne D.; Clark, Ezra; Tsai, Charlie; Hahn, Christopher; Jaramillo, Thomas F.; Chan, Karen; Bell, Alexis T. Promoter Effects of Alkali Metal Cations on the Electrochemical Reduction of Carbon Dioxide. *J. Am. Chem. Soc.* **2017**, *139* (32), 11277–11287. https://doi.org/10.1021/jacs.7b06765.

(26) Effect of Counterion Size on Short Range Repulsive Forces at High Ionic Strengths, Miroslav Colic, George V. Franks, Matthew L. Fisher, and Fred F. Lange, Langmuir 1997 13 (12), 3129-3135, DOI: 10.1021/la960965p

(27) Smekal, Werner; Werner, Wolfgang S. M.; Powell, Cedric J. Simulation of Electron Spectra for Surface Analysis (SESSA): A Novel Software Tool for Quantitative Auger-Electron Spectroscopy and X-Ray Photoelectron Spectroscopy. *Surf. Interface Anal.* **2005**, *37* (11), 1059–1067. https://doi.org/10.1002/sia.2097

(28) Weatherup, Robert S.; Eren, Baran; Hao, Yibo; Bluhm, Hendrik; Salmeron, Miquel B. Graphene Membranes for Atmospheric Pressure Photoelectron Spectroscopy. *J. Phys. Chem. Lett.* **2016**, *7* (9), 1622–1627. https://doi.org/10.1021/acs.jpclett.6b00640.

(29) Lu, Yi-Hsien; Larson, Jonathan M.; Baskin, Artem; Zhao, Xiao; Ashby, Paul D.; Prendergast, David; Bechtel, Hans A.; Kostecki, Robert; Salmeron, Miquel. Infrared Nanospectroscopy at the Graphene–Electrolyte Interface. *Nano Lett.* **2019**, *19* (8), 5388–5393. https://doi.org/10.1021/acs.nanolett.9b01897.

(30) Mean Free Paths and Cross Sections for Electron Scattering from Liquid Water, Nidhi Sinha and Bobby Antony, The Journal of Physical Chemistry B 2021 125 (21), 5479-5488, DOI: 10.1021/acs.jpcb.0c10781

(31) Kokalj, Anton. On the Use of the Langmuir and Other Adsorption Isotherms in Corrosion Inhibition. *Corros. Sci.* **2023**, *217* (December 2022), 111112. https://doi.org/10.1016/j.corsci.2023.111112.

(32) Nong, Hong Nhan; Falling, Lorenz J.; Bergmann, Arno; Klingenhof, Malte; Tran, Hoang Phi; Spöri, Camillo; Mom, Rik; Timoshenko, Janis; Zichittella, Guido; Knop-Gericke, Axel; Piccinin, Simone; Pérez-Ramírez, Javier; Cuenya, Beatriz Roldan; Schlögl, Robert; Strasser, Peter; Teschner, Detre; Jones, Travis E. Key Role of Chemistry versus Bias in Electrocatalytic Oxygen Evolution. *Nature* **2020**, *587* (7834), 408–413. https://doi.org/10.1038/s41586-020-2908-2.

(33) Van-Thai Pham, John L. Fulton, Contact ion-pair structure in concentrated cesium chloride aqueous solutions: An extended X-ray absorption fine structure study,Journal of Electron Spectroscopy and Related Phenomena,Volume 229,2018,Pages 20-25,https://doi.org/10.1016/j.elspec.2018.09.004.

(34) Linking Electric Double Layer Formation to Electrocatalytic Activity, Matthew A. Gebbie, Beichen Liu, Wenxiao Guo, Seth R. Anderson, and Samuel G. Johnstone, ACS Catalysis 2023 13 (24), 16222-16239, DOI: 10.1021/acscatal.3c04255

(35) Aqueous Solution/Air Interfaces Probed with Sum Frequency Generation Spectroscopy, Mary Jane Schultz, Steve Baldelli, Cheryl Schnitzer, and Danielle Simonelli, The Journal of Physical Chemistry B 2002 106 (21), 5313-5324, DOI: 10.1021/jp014466v

(36) Henke, B. L.; Gullikson, E. M.; Davis, J. C. X-Ray Interactions: Photoabsorption, Scattering, Transmission, and Reflection at E = 50-30, 000 EV, Z = 1-92. *Atomic Data and Nuclear Data Tables*. 1993, pp 181–342. https://doi.org/10.1006/adnd.1993.1013.

(37) Salmeron, Miquel B.; Schlögl, Robert. Ambient Pressure Photoelectron Spectroscopy: A New Tool for Surface Science and Nanotechnology. *Surf. Sci. Rep.* **2008**, *63* (4), 169–199. https://doi.org/10.1016/j.surfrep.2008.01.001.

(38) Liangzhi Zhou, Laura Fox, Magdalena Włodek, Luisa Islas, Anna Slastanova, Eric Robles, Oier Bikondoa, Robert Harniman, Neil Fox, Mattia Cattelan, Wuge H. Briscoe, Surface structure of few layer graphene, Carbon, Volume 136, 2018, Pages 255-261, https://doi.org/10.1016/j.carbon.2018.04.089.

(39) Lin, Yung Chang; Lu, Chun Chieh; Yeh, Chao Huei; Jin, Chuanhong; Suenaga, Kazu; Chiu, Po Wen. Graphene Annealing: How Clean Can It Be? *Nano Lett.* **2012**, *12* (1), 414–419. https://doi.org/10.1021/nl203733r.

(40) Mähler, Johan; Persson, Ingmar. A Study of the Hydration of the Alkali Metal Ions in Aqueous Solution. *Inorg. Chem.* **2012**, *51* (1), 425–438. https://doi.org/10.1021/ic2018693.

(41) Velasco-Velez, J. J.; Wu, C. H.; Pascal, Tod A.; Wan, Liwen F.; Guo, Jinghua; Prendergast, David; Salmeron, Miquel. The Structure of Interfacial Water on Gold Electrodes Studied by X-Ray Absorption Spectroscopy. *Science* **2014**, *346* (6211), 831–834. https://doi.org/10.1126/science.1259437.

(42) Schön, Daniela; Xiao, Jie; Golnak, Ronny; Tesch, Marc F.; Winter, Bernd; Velasco-Velez, Juan-Jesus; Aziz, Emad F. Introducing Ionic-Current Detection for X-Ray Absorption Spectroscopy in Liquid Cells. *J. Phys. Chem. Lett.* **2017**, *8* (9), 2087–2092. https://doi.org/10.1021/acs.jpclett.7b00646.

(43) Van Spronsen, Matthijs A.; Zhao, Xiao; Jaugstetter, Maximilian; Escudero, Carlos; Duchoň, Tomáš; Hunt, Adrian; Waluyo, Iradwikanari; Yang, Peidong; Tschulik, Kristina; Salmeron, Miquel B. Interface Sensitivity in Electron/Ion Yield X-Ray Absorption Spectroscopy: The TiO2-H2O Interface. *J. Phys. Chem. Lett.* **2021**, *12* (41), 10212–10217. https://doi.org/10.1021/acs.jpclett.1c02115.

(44) Henke, B. L.; Gullikson, E. M.; Davis, J. C. X-Ray Interactions: Photoabsorption, Scattering, Transmission, and Reflection at E = 50-30, 000 EV, Z = 1-92. *Atomic Data and Nuclear Data Tables*. 1993, pp 181–342. https://doi.org/10.1006/adnd.1993.1013.

(45) https://doi.org/10.2172/4545040

(46) https://dx.doi.org/10.18434/T4D01F

(47) Bonanni, Alessandra; umera, Martin. High-Resolution Impedance Spectroscopy for Graphene Characterization. *Electrochem. commun.* **2013**, *26* (1), 52–54. https://doi.org/10.1016/j.elecom.2012.10.013.

(48) Angizi, Shayan; Hong, Lea; Huang, Xianxuan; Selvaganapathy, P. Ravi; Kruse, Peter. Graphene versus Concentrated Aqueous Electrolytes: The Role of the Electrochemical Double Layer in Determining the Screening Length of an Electrolyte. *npj 2D Mater. Appl.* **2023**, *7* (1), 67. https://doi.org/10.1038/s41699-023-00431-y.

(49) Pajkossy, Tamás; Wandlowski, Thomas; Kolb, Dieter M. Impedance Aspects of Anion Adsorption on Gold Single Crystal Electrodes. *J. Electroanal. Chem.* **1996**, *414* (2), 209–220. https://doi.org/10.1016/0022-0728(96)04700-6.

(50) Stieble, M.; Jüttner, K. Surface Blocking in the Redox System Pt/[Fe(CN)6]3−,[Fe(CN)6]4−. *J. Electroanal. Chem. Interfacial Electrochem.* **1990**, *290* (1–2), 163–180. https://doi.org/10.1016/0022-0728(90)87428-M.

(51) Choi, Woosung; Shin, Heon-Cheol; Kim, Ji Man; Choi, Jae-Young; Yoon, Won-Sub. Modeling and Applications of Electrochemical Impedance Spectroscopy (EIS) for Lithium-

Ion Batteries. *J. Electrochem. Sci. Technol.* **2020**, *11* (1), 1–13. https://doi.org/10.33961/jecst.2019.00528.

.

(52) Williams, Christopher D.; Dix, James; Troisi, Alessandro; Carbone, Paola. Effective Polarization in Pairwise Potentials at the Graphene-Electrolyte Interface. *J. Phys. Chem. Lett.* **2017**, *8* (3), 703–708. https://doi.org/10.1021/acs.jpclett.6b02783.

(53) Zhan, Cheng; Cerón, Maira R.; Hawks, Steven A.; Otani, Minoru; Wood, Brandon C.; Pham, Tuan Anh; Stadermann, Michael; Campbell, Patrick G. Specific Ion Effects at Graphitic Interfaces. *Nat. Commun.* **2019**, *10* (1), 1–8. https://doi.org/10.1038/s41467-019-12854-7.

(54) Marcus, Yizhak. Effect of Ions on the Structure of Water. *Pure Appl. Chem.* **2010**, *82* (10), 1889–1899. https://doi.org/10.1351/PAC-CON-09-07-02.

(55) J V Joshi *et al* 2007 *J. Phys.: Condens. Matter* **19** 196219

(56) Benoît Schnell, Rachel Schurhammer, and Georges Wipff,*The Journal of Physical Chemistry, B* **2004** *108* (7), 2285-2294 ,DOI: 10.1021/jp036896m

(57) Serva A, Havenith M, Pezzotti S. The role of hydrophobic hydration in the free energy of chemical reactions at the gold/water interface: Size and position effects. J Chem Phys. 2021 Nov 28;155(20):204706. doi: 10.1063/5.0069498

(58) Lee, Alpha A.; Perez-Martinez, Carla S.; Smith, Alexander M.; Perkin, Susan. Scaling Analysis of the Screening Length in Concentrated Electrolytes. *Phys. Rev. Lett.* **2017**, *119* (2), 026002. https://doi.org/10.1103/PhysRevLett.119.026002.

(59) Gaddam, Prudhvidhar; Ducker, William. Electrostatic Screening Length in Concentrated Salt Solutions. *Langmuir* **2019**, *35* (17), 5719–5727. https://doi.org/10.1021/acs.langmuir.9b00375.

(60) Baldelli, Steve; Schnitzer, Cheryl; Shultz, Mary Jane; Campbell, D. J. Sum Frequency Generation Investigation of Water at the Surface of H OrH SO and H OrCs SO Binary Systems 2 2 4 2 2 4. *Chem. Phys. Lett.* **1998**, *287* (April), 143–147.

(61) Han Seung Lee, Manickam Adhimoolam Arunagirinathan, Apostolos Vagias, Sangwoo Lee, Jayesh R. Bellare, H. Ted Davis, Eric W. Kaler, Alon V. McCormick, and Frank S. Bates *Langmuir* **2014** *30* (43), 12743-12747
DOI: 10.1021/la502809y

(62) Schmickler, Wolfgang. The Effect of Weak Adsorption on the Double Layer Capacitance. *ChemElectroChem* **2021**, *8* (22), 4218–4222. https://doi.org/10.1002/celc.202100842.

(63) Doblhoff-Dier, Katharina; Koper, Marc T. M. Modeling the Gouy-Chapman Diffuse Capacitance with Attractive Ion-Surface Interaction. *J. Phys. Chem. C* **2021**, *125* (30), 16664–16673. https://doi.org/10.1021/acs.jpcc.1c02381.

(64) Bu, Wei; Vaknin, David; Travesset, Alex. How Accurate Is Poisson-Boltzmann Theory for Monovalent Ions near Highly Charged Interfaces? *Langmuir* **2006**, *22* (13), 5673–5681. https://doi.org/10.1021/la053400e.

(65) Lee, Alpha A.; Perez-Martinez, Carla S.; Smith, Alexander M.; Perkin, Susan. Scaling Analysis of the Screening Length in Concentrated Electrolytes. *Phys. Rev. Lett.* **2017**, *119* (2), 026002. https://doi.org/10.1103/PhysRevLett.119.026002.

(66) Fisher, F.H., Fox, A.P. $LiSO^-_4$, $RbSO^-_4$, $CsSO^-_4$, and $(NH_4)SO^-_4$ ion pairs in aqueous solutions at pressures up to 2000 atm. *J Solution Chem* **7**, 561–570 (1978). https://doi.org/10.1007/BF01074872

(67) Qin, X., Hansen, H.A., Honkala, K. *et al.* Cation-induced changes in the inner- and outer-sphere mechanisms of electrocatalytic CO_2 reduction. *Nat Commun* **14**, 7607 (2023). https://doi.org/10.1038/s41467-023-43300-4